Accident Analysis and Prevention 157 (2021) 106172

Contents lists available at ScienceDirect

Accident Analysis and Prevention

journal homepage: www.elsevier.com/locate/aap

Formulating a GIS-based geometric design quality assessment model for Mountain highways

Hong Zhang [a,b], Min Zhang [c,*], Chi Zhang [a,b], Lei Hou [d]

[a] Key Laboratory for Special Area Highway Engineering of Ministry of Education, Chang'an University, Xi'an, 710064, Shaanxi, China
[b] Engineering Research Center of Highway Infrastructure Digitalization, Ministry of Education, Xi'an, 710000, Shaanxi, China
[c] College of Transportation Engineering, Chang'an University, Xi'an, 710064, Shaanxi, China
[d] School of Engineering, RMIT University, Melbourne, 3000, Victoria, Australia

ARTICLE INFO

Keywords:
Mountainous highways
Road traffic safety
GIS
FTA
DEMATEL
GDQ

ABSTRACT

Highways play an important role in China's economic development, especially in mountainous regions. In reality, design of mountainous highways can be a challenging task due to complex geological and topographic conditions. From the safety perspective, it is also important that road geometric design defects and potential accident blind spots can be reasonably identified from the design. To this end, this study formulated an innovative Geographic Information System (GIS)-based geometric design quality assessment model for mountain highways. First, a fault tree analysis (FTA) was conducted to identify a series of highway design risk factors. Second, a decision-making trial and evaluation laboratory (DEMATEL) technique was employed to derive the factors' weight and sensitivity. Third, road driving suitability, traffic safety sensitivity, design risk factors, and effective distance were taken into account to formulate a design quality assessment model. Forth, two case studies based on a mountainous highway located in southwest China were conducted to validate this model. The case studies established that improving geometric design quality can significantly improve the road traffic safety of mountainous highways. It is also revealed that the existence of steep slopes, tunnels, and rapid horizontal and vertical alignment change can considerably compromise the geometric design quality (GDQ), therefore, configuring these parameters is worth of further investigation. Last but not least, this study provides essential knowledge to the regime of accident prevention, high-risk road section location and mapping, traffic safety management, and design of smart transport systems.

1. Introduction

By rough estimate, about two-thirds of the total area of China consists of mountains. Especially, the southwest regions of China possess complex landforms and geological conditions (Wang and Prato, 2019). Development of road projects in these areas can significantly improve their overall accessibility, reduce transportation costs, and increase productivity and economy. Design of road infrastructure involves many complex factors that can compromise road traffic safety, such as speeding (Intini et al., 2020), fatigue (Watling et al., 2016), poor visibility (Li et al., 2019; Colonna et al., 2020), vehicle friction and skid (Chen et al., 2012; Colonna et al., 2016, 2017; Pitaksringkarn et al., 2018; Wang et al., 2019), brake failure (Zhang et al., 2019), speed dispersion (Yan et al., 2019), fickle weather conditions (Zhang et al., 2015b; Ashley et al., 2015), and so on. According to the National Bureau of Statistics (2019), over seventy thousand mountainous regions accidents were recorded in China in 2018, leading to over a hundred thousand casualties and losses of millions of dollars.

According to Wen et al. (2016) and Zhang et al. (2017), highway geometric design quality (GDQ) must take into account the aforementioned factors. Currently, the most common GDQ evaluation methods are highway safety auditing and geometric design consistency check. Over a hundred countries have formulated different safety auditing and design consistency check techniques (World Health Organization, 2015). A geometric design consistency check focuses on the analysis of difference between driver expectation and road design specifications. Overall, the greater the difference, the higher the crash rate (Meng et al., 2011; Luque and Castro, 2016; Wang et al., 2017; Wang and Prato, 2019; Llopis-Castello et al., 2019).

Nowadays, numerous approaches have been formulated to evaluate

* Corresponding author at: Middle Section of the South Second Ring Road, Yanta District, Xi'an, 710064, Shaanxi, China.
E-mail addresses: hongzhang@chd.edu.cn (H. Zhang), minzhang@chd.edu.cn (M. Zhang), zhangchi@chd.edu.cn (C. Zhang), lei.hou@rmit.edu.au (L. Hou).

https://doi.org/10.1016/j.aap.2021.106172
Received 21 December 2020; Received in revised form 27 March 2021; Accepted 2 May 2021
Available online 10 May 2021
0001-4575/© 2021 Elsevier Ltd. All rights reserved.

highway GDQ and the synergistic effects of roads, vehicles, drivers, and environmental impact on accidents. These approaches incorporate, but are not limited to, statistical analysis (Abdelrahman et al., 2018), clustering analysis (Naji et al., 2020; Xiong et al., 2019), fuzzy logic (Ani et al., 2019; Cai et al., 2005), deep learning (Ping et al., 2018; Shah et al., 2017), driving risk field theory (Wang et al., 2016), reliability theory (Sun and You, 2013), extension science model (Zhang et al., 2016), Bayesian model (Ma et al., 2019), Logit regression model (Naji et al., 2018), negative binomial regression model (Meng et al., 2012), and so on. Accidents and near-misses can be affected by highway design risk factors such as curve radius projected to the horizontal plane, longitudinal gradient, deflection angles, roadway width, and superelevation. Wang and Prato (2019) formulated a partial proportional odds model to analyse how these factors influenced the severity of traffic accidents. This study evidenced that mountainous highways should reduce the use of sharp turns, long curves, and steep slopes as much as possible. Li and He (2016) established a closed-loop drive-vehicle-road-environment system to analyse the influence of curve radius and superelevation rate on lateral tire force, revealing that both radius and superelevation rate safety margin should be increased to accommodate safety requirements. Zhang et al. (2015a) looked into road curve sideslip risks using Carsim, which found that curve radius is a more important factor in road traffic safety.

A Geographic Information System (GIS) is a computer system for capturing, storing, checking, and displaying data related to positions on Earth's surface. It can create digital cartographic resources, link road attributes to spatial data, handle big data, and present spatiotemporal feature maps (Budzynski et al., 2018). GIS approaches have been widely used to analyse the spatial distribution of traffic accidents and accident-prone road networks, including hotspot analysis (Getis-Ord Gi*), high/low clustering (Getis-Ord General G), spatial autocorrelation (Morans I), Kernel Density Estimation (KDE), and so on. Ciobanu and Benedek (2015) implemented KDE and derived a set of accident distribution maps, evidencing that road intersections would always be more accident-prone. Kara and Akcit (2015) conducted a spatial autocorrelation and hot spot analysis and formulated a number of driving risk reduction measures for road intersections.

Despite risk-associated mechanisms have been well studied, mountainous road design is still a challenging research topic when considering its spatial distribution, longitudinal gradient, slope length, and horizontal and vertical alignment change. Most previous highway GDQ techniques relied on traffic accident data, travel speed, and geometric design schemes obtained from fitting satellite images (Farahmand and Boroujerdian, 2018), high-resolution laser scanning data (Sameen and Pradhan, 2017), GPS data (Zainal et al., 2017), and Google Earth (Wang and Prato, 2019). However, acquiring and processing a wide range of datasets from multiple sources could be very tedious. To efficiently identify the geometric design defects and accident-prone road sections in mountainous highways, this paper formulated a novel GIS-based GDQ assessment model based on a three-step method, namely, using the fault tree analysis (FTA) technique to identify the highway design risk factors, using the decision-making trial and evaluation laboratory (DEMATEL) technique to analyse each identified factor's weight and sensitivity, and formulating a model that incorporates a wide range of road design factors. Finally, two case studies were conducted to validate the model efficacy.

2. Methodology

2.1. Identifying the highway design related risk factors

FTA is a top-down deductive failure analysis method that can be used to derive the causality of system failure and its likely reasons (Chen et al., 2018; Li et al., 2019). In this study, an FTA was conducted to examine multiple road design related factors that contributed to over two thousand traffic accidents recorded in the southwest China mountainous regions between 2013 and 2017. The analysed accidents did not include the ones associated with drink/drunk driving, unlicensed driving, drug driving, etc. In our study, the fault tree was designed to include three levels (Fig. A1). The top level collated the traffic accident records and the intermediate and bottom levels contained the direct and indirect causes of these accidents. The highway design related risk factors were summarised through analysing the indirect causes from the fault tree (Table 1). As these factors possess different units, values, and risk impact, they need to be normalised prior to denoting the threat intensity (Table A1) (AASHTO, 2018; Ministry of Transport of the People's Republic of China, 2015).

Table 1
Highway design risk factors.

No.	Factor	Numeric Annotation	Feature
1	*Li: Lighting design in tunnel*	Tunnel lighting reflectors only (1); General lighting system only (2); Enhanced lighting system & general lighting system (3)	Global multiple
2	*Ln: Tunnel length (m)*	decimal	Local continuous
3	*Lt: Tangent length (m)*	decimal	Local continuous
4	*Ri: curve radius projected to the horizontal plane (m)*	decimal	Local continuous
5	*μ: Lateral force coefficient*	related to speed, horizontal curve radius, and superelevation, decimal	Local continuous
6	*Ls: Transition curve length (m)*	decimal	Local continuous
7	*Lh: Horizontal curve length (m)*	horizontal & tangent-to-curve transition curves (length total), decimal	Local continuous
8	*G: Longitudinal grade (%)*	decimal	Local continuous
9	*Lp: Slope length (m)*	decimal	Local continuous
10	*Rci: Crest curve radius projected to the vertical plane (m)*	decimal	Local continuous
11	*Rsi: Sag curve radius projected to the vertical plane (m)*	decimal	Local continuous
12	*Lv: Vertical curve length (m)*	decimal	Local continuous
13	*Tf: Traffic engineering and roadside facilities*	irregular design (1); poor visibility (2); standard design & good visibility (3)	Global multiple
14	*Em: Emergency escape ramps*	poor design (1); inappropriate position (2); standard design & appropriate position (3)	Global multiple
15	*D: Roadside conditions*	no guardrails (1); dull landscape (2); guardrails & nice landscape (3)	Global multiple
16	*Q: Traffic volume (pcu/(h'ln))*	the number of standard vehicles per lane per hour, integer	Local continuous
17	*Ric: Horizontal alignment change (m)*	change in curve radius projected to the horizontal plane, decimal	Local continuous
18	*Gc: Vertical alignment change (%)*	change in longitudinal grade, decimal	Local continuous
19	*Wc: Cross-section change*	change in cross-section width: narrowing (1); widening (2); no change (3)	Global multiple
20	*A: Tunnel entrance or exit*	within 200 m away from a tunnel entrance (1) or exit (2)	Global multiple

It is indicated from the FTA that driving fatigue, speeding, brake failure, lateral instability, and poor visibility are the most frequent direct risk factors. On downhill roads, continuous brake will increase the brake disc temperature and reduce the friction coefficient, which may lead to brake failure and serious consequences. Lateral instability refers to the horizontal instability caused by larger lateral force coefficient, shorter transition curve or horizontal curve length (Rosey and Auberlet, 2012; Zhang et al., 2015a), as well as the longitudinal instability resulted from

Table 2
Demonstration of the DEMATEL results.

No.	Factors	Symbols	f_i	g_j	m_i	n_i	w_i	S_i
1	Lighting design in tunnel	*Li*	0	0.25	0.250	−0.25	0.562	0.438
2	Tunnel length (m)	*Ln*	0.443	0	0.443	0.443	0.609	0.609
3	Tangent length (m)	*Lt*	0.281	0	0.281	0.281	0.57	0.57
4	Curve radius projected to the horizontal plane (m)	*Ri*	0.882	0.29	1.172	0.591	0.764	0.644
5	Lateral force coefficient	*μ*	0	0.427	0.427	−0.427	0.605	0.395
6	Transition curve length (m)	*Ls*	0.173	0.29	0.463	−0.118	0.614	0.471
7	Horizontal curve length (m)	*Lh*	0.382	0.323	0.704	0.059	0.669	0.515
8	Longitudinal grade (%)	*G*	0.547	0.411	0.958	0.136	0.723	0.534
9	Slope length (m)	*Lp*	0.25	0.176	0.426	0.074	0.605	0.518
10	Crest curve radius projected to the vertical plane (m)	*Rci*	0.375	0.125	0.5	0.250	0.622	0.562
11	Sag curve radius projected to the vertical plane (m)	*Rsi*	0.375	0.125	0.5	0.250	0.622	0.562
12	Vertical curve length (m)	*Lv*	0	0.281	0.281	−0.281	0.57	0.43
13	Traffic engineering and roadside facilities	*Tf*	0	1.84	1.84	−1.84	0.863	0.137
14	Emergency escape ramps	*Em*	0	0.766	0.766	−0.766	0.683	0.317
15	Roadside conditions	*D*	0.25	0.125	0.375	0.125	0.593	0.531
16	Traffic volume (pcu/(h'ln))	*Q*	0.25	0	0.25	0.25	0.562	0.562
17	Horizontal alignment change (m)	*Ric*	0.125	0.161	0.286	−0.036	0.571	0.491
18	Vertical alignment change (%)	*Gc*	0.125	0.176	0.301	−0.051	0.575	0.487
19	Cross-section change	*Wc*	0.125	0.125	0.25	0	0.562	0.5
20	Tunnel entrance or exit	*A*	1.31	0	1.31	1.31	0.787	0.787

shorter vertical curve length or steep slope (Hu et al., 2010). Moreover, inconsistent geometric design may also lead to lateral instability accidents (Li et al., 2019; Intini et al., 2020), such as rapid changes in horizontal alignment, vertical alignment, or cross-section areas. Driving visibility can be affected by road geometric features as well, for instance, sharp turns, a swift drop of heigh, changing brightness, concealed roads, lack of traffic lights, and so on (Yan et al., 2011; Zhang, 2020).

2.2. Determining the risk factor weight and safety sensitivity

DEMATEL is a well-proven method to disclose the rationale of complex clusters that of various links and standards (Cui et al., 2013), therefore, it was used in our study to determine the risk factors' weights and the sensitivity level of traffic safety on each factor. In view that the risk factors are not independent and may affect one another, a DEMATEL method was implemented through determining the mutual relation between pairwise risk factors, calculating the relative importance/net effect of each risk factor, and normalising the relative importance/net effect to obtain each risk factor's weight and safety sensitivity.

(1) To evaluate the relationship among the risk factors, a direct-relation matrix (Z), a normalised direct-relation matrix (X) and a total-relation matrix (T) were formulated using Eqs. (1)–(3) (these matrixes can be referred to from the Appendices).

$$Z=(z_{ij})_{n\times n} \tag{1}$$

$$X=\left(x_{ij}\right)_{n\times n}=\frac{1}{\max\sum_{j=1}^{n}z_{ij}}\times Z \tag{2}$$

$$T=\left(t_{ij}\right)_{n\times n}=\lim_{k\to\infty}\left(X+X^2+\ldots+X^k\right)=X(I-X)^{-1} \tag{3}$$

where z_{ij} represents the influence of the ith factor on the jth factor (set to 1 if the influence was present or 0 if not). I represents the identity matrix (i.e., the self-influence factor). Its main diagonal element values are set to 1 and the rest 0.

(2) To obtain each risk factor's relative importance/net effect, the distributing influence (f_i) and the receiving influence (g_j) were calculated using Eq.s (4)–(5). These values are the totals of the matrix (T)'s ith row and jth column and reflect the direct and indirect influence of the ith factor on the other factors, as well as the direct and indirect influence of the jth factor received from the other factors. The relative importance (m_i) and the net effect (n_i) were calculated using Eq.s (6)–(7). The former represents the position of the ith factor in the system (note a larger value indicates a closer relationship with the other factors and a higher weight), and the latter classifies the causal factors (positive values) and the resultant factors (negative values) (note traffic safety is more sensitive to the causal factors (Yazdi et al., 2020), and a larger value indicates the risk factor has greater influence over the other factors).

$$f_i=\sum_{j=1}^{n}t_{ij} \tag{4}$$

$$g_j=\sum_{i=1}^{n}t_{ij} \tag{5}$$

$$m_i=f_i+g_j \tag{6}$$

$$n_i=f_i-g_j \tag{7}$$

(3) To obtain the ith factor's weight (w_i) and the sensitivity level of traffic safety on ith factor (S_i), the relative importance (m_i) and the net effect (n_i) were normalised through the Sigmoid function (Lipovetsky, 2010), according to Eqs. (8)–(9).

$$w_i=\frac{1}{1+e^{-m_i}} \tag{8}$$

$$S_i=\frac{1}{1+e^{-n_i}} \tag{9}$$

The DEMATEL results showed that the factor of traffic engineering and roadside facilities closely relate to the other factors (m_i = 1.84), followed by tunnel entrance or exit (m_i = 1.31), curve radius (m_i = 1.172), longitudinal grade (m_i = 0.958), just to list a few. (Table 2). Tunnel lighting design, traffic volume, and cross-section changes loosely relate to the other factors, as evidenced from m_i = 0.25. The causal factors were then identified as tunnel length, tangent length, curve radius projected to the horizontal plane, horizontal curve length, longitudinal grade, slope length, crest curve radius projected to the vertical plane, sag curve radius projected to the vertical plane, roadside design, traffic volume, and tunnel entrance or exit (n_i>0), to which a typical road design practice should pay attention as well.

2.3. GDQ assessment model

In this study, the driving risk related to a number of factors which involve risk weight, risk threat intensity spatial distribution, distance

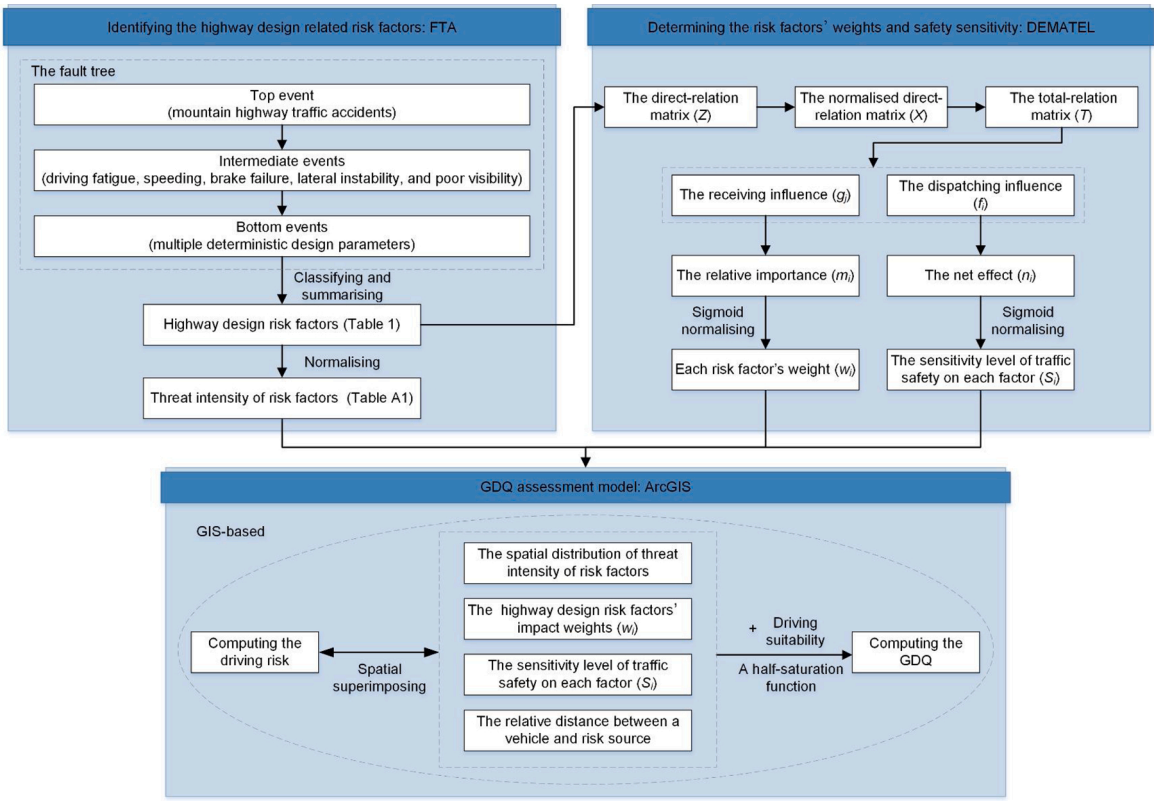

Fig. 1. Flowchart of formulating the GDQ assessment model.

between a vehicle and a risk source, and traffic safety relative sensitivity. Eventually, the spatial distribution of driving risk and GDQ can be calculated by adding up the risk factor influence (Fig. 1).

As the driving risk and GDQ assessment involved spatial distribution and distance calculation, they were generated using GIS analysis and statistics techniques. The GIS-based implementation process is as follows:

(1) The two-dimensional coordinates of each station point (XY data) on the road centerline were displayed on the geospatial map and then plotted onto the base raster map.
(2) Likewise, the values of the design parameters at each station point (risk factors distribution data) were displayed on the geospatial map and then plotted onto a series of threat raster maps. The grid cell values in these maps reflected the threat intensity (Table A1).
(3) The threat raster maps were then superposed to generate the driving risk map, according to Eq. (10).

$$R_x = \sum_{i=1}^{i} \sum_{y=1}^{y_i} \left(\frac{w_i}{\sum_{i=1}^{i} w_i} \right) i_y D_{ixy} S_i \tag{10}$$

where R_x represents the xth grid cell's driving risk of the base raster map. y_i represents the grid cells entirety on threat r's raster map. w_i represents risk factor r's weight (ranging from 0 to 1), and the normalised weight was used to rate the mean driving risk. i_y represents the yth grid cell's threat intensity (ranging from 0 to 1) on threat r's raster map. As the grid cells closer to the risk source were more affected (Wu et al., 2014), the yth grid cell's distance-decay influence on the xth grid cell, expressed as D_{ixy}, can be expressed as a linear function and an exponential function (Eqs. (11) and (12)). S_i represents the relative sensitivity of traffic safety on each risk factor (ranging from 0 to 1), and a larger value means a section is more risk-prone.

$$D_{ixy} = 1 - \frac{d_{xy}}{d_{r\max}} \tag{11}$$

$$D_{ixy} = \exp\left(-\frac{\alpha}{d_{r\max}} d_{xy} \right) \tag{12}$$

where d_{xy} represents the linear distance between xth grid cell and yth grid cell. $d_{r\max}$ represents the maximum effective distance, i.e., 400 m, that a risk factor r could reach (Chen et al., 2020). α is the exponential function coefficient and its default value was set to 2.99 (Zhang et al., 2020b).

(4) A half-saturation function, expressed as Eq. (13), was used to convert the grid cell risk scoring to GDQ. This function only redistributes the spread and centering trend of the grid cell's driving risk score (Mulder and Hendriks, 2014). The higher the GDQ, the smoother the road section.

$$GDQ_x = A\left(1 - \frac{R_x^z}{R_x^z + k^z} \right) \tag{13}$$

where GDQ_x represents the xth grid cell's GDQ on the base raster map. A represents the driving suitability of a road (ranging from 0 to 1) and its value was set to 0.7 for mountain highways. Z is a constant and its value was set to 2.5. k is the scaling parameter, and its default value was set to 0.5, which is the maximum score out of the raster maps. Therefore, the GDQ values ranged between 50 %A and $A_{\max}$. Fig. 2 presents an entire GIS-based process of the study adapted from Zhang et al. (2020a). A comparison of the formulated model with other models was made in Table 3, which reveals the model sweeping advantages in terms of accurately generating GDQ spatial distribution maps for a wide range of road types.

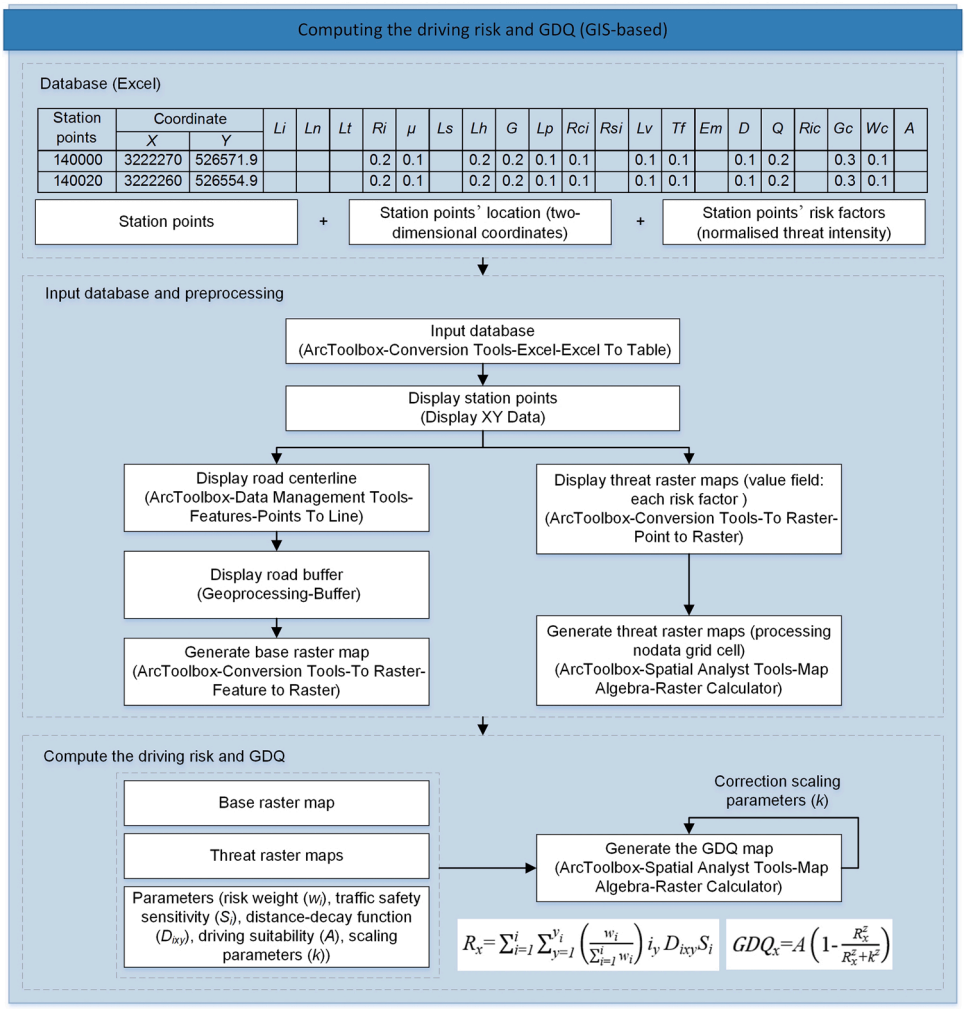

Fig. 2. GIS-based GDQ map generation process (adapted from Zhang et al., 2020a).

Table 3
Comparison of the prevalent GDQ evaluation methods.

Methods	Required data	Evaluation results	Efficiency	Applicability
Highway safety auditing	Road design data	Checklist with qualitative results	Manual audit, time-consuming	Broader road types
Accident-based geometric design consistency check	Accidents	Accident blind spots	Acquiring accidents, time-consuming	Operating roads
Speed-based geometric design consistency check	Measured or predicted speed	Road sections with large speed gradients	Acquiring speed, time-consuming	Broader road types
Proposed GDQ assessment model	Road design data	GDQ map	GIS-based semi-automation	Broader road types

3. Case studies

3.1. Study sections and data preparation

The proposed model was applied to the road sections of G5 in between 140 km and 160 km (Case 1) and 95 km and 115 km (Case 2) (Fig. 3a). There were 185 accidents and 266 accidents being recorded in these sections from 2013 to 2017. Fig. 3b and c show the designed horizontal and vertical alignments of the sections. In Case 1, there is a spiral up section in Tunnel 2, i.e., between 151.880 km and 153.683 km. More design specifications retrieved from our survey on the road designers can be referred to from Table 4. The coordinates of each station point at an interval of 20 m along the road centerline and their design parameters were retrieved from the geometric design scheme. Then the corresponding base raster map and threat raster maps were generated from GIS conversion, data management, geoprocessing and spatial analysis tools (Fig. A2). Next, the GDQ distribution was mapped out using the GIS raster calculator (Fig. 4). Finally, the model was validated by examining the relationship of GDQ and accidents.

3.2. GDQ evaluation results

It can be seen from Fig. 4 that the GDQ spatial distribution varied substantially. In Case 1, lower GDQ values were observed in between 151.02 and 152.5 km, and 154.4 and 156.1 km, namely, within the 800 m range of the two ends of the tunnel. The lowest GDQ value scored at 0.35 and appeared at the 155.68 km kilometric point. The straight line between the curves of the opposite turns is 121.194 m long with a longitudinal grade being 3.66 % and crest curve radius (projected to the vertical plane) being 40 km. A higher accident rate was witnessed within the 400 m range of this point, despite there was an emergency escape ramp. Higher GDQ values were observed in between 140 and 140.84

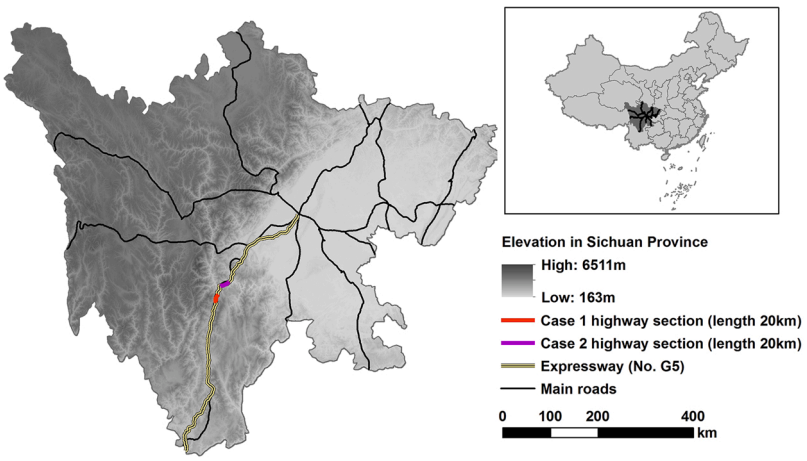

(a)

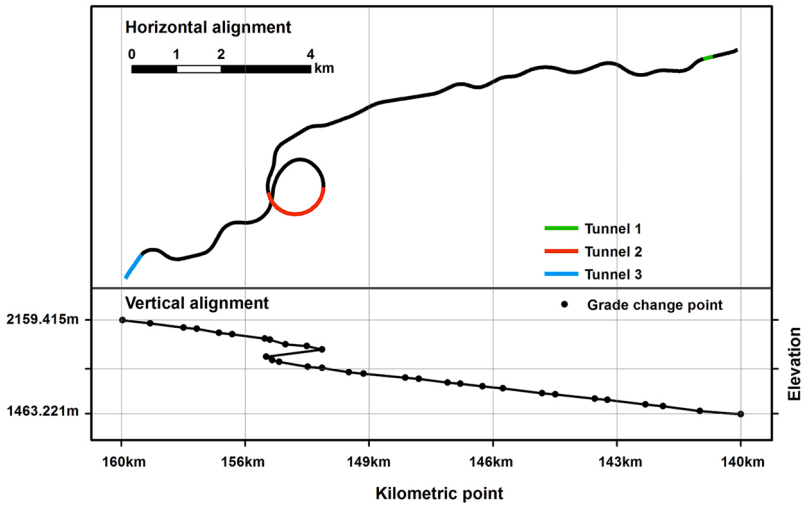

(b)

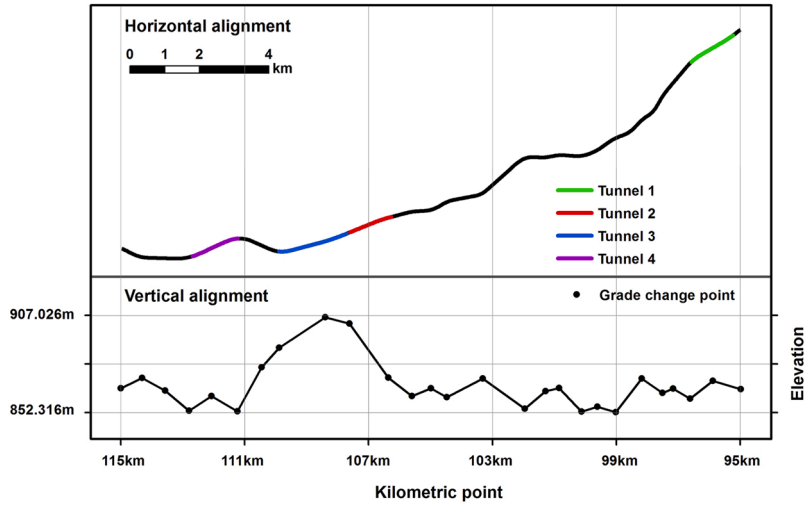

(c)

Fig. 3. (a) Section overview; (b) Case 1 alignment; (c) Case 2 alignment.

Table 4
Basic information of two cases.

Design Specifications	Case 1	Case 2
Design speed (km/h)	80	80
Annual average daily traffic (AADT) (pcu/d)	13,937	20,774
Elevation difference between the highest and lowest points (m)	696.194	54.710
Maximum average longitudinal grade (%)	3.48	0.60
Minimum curve radius projected to the horizontal plane (m)	335	600
Maximum longitudinal grade (%)	4.95	3.978
Number of crashes	185 (1.85/kilometer/year)	266 (2.66/kilometer/year)

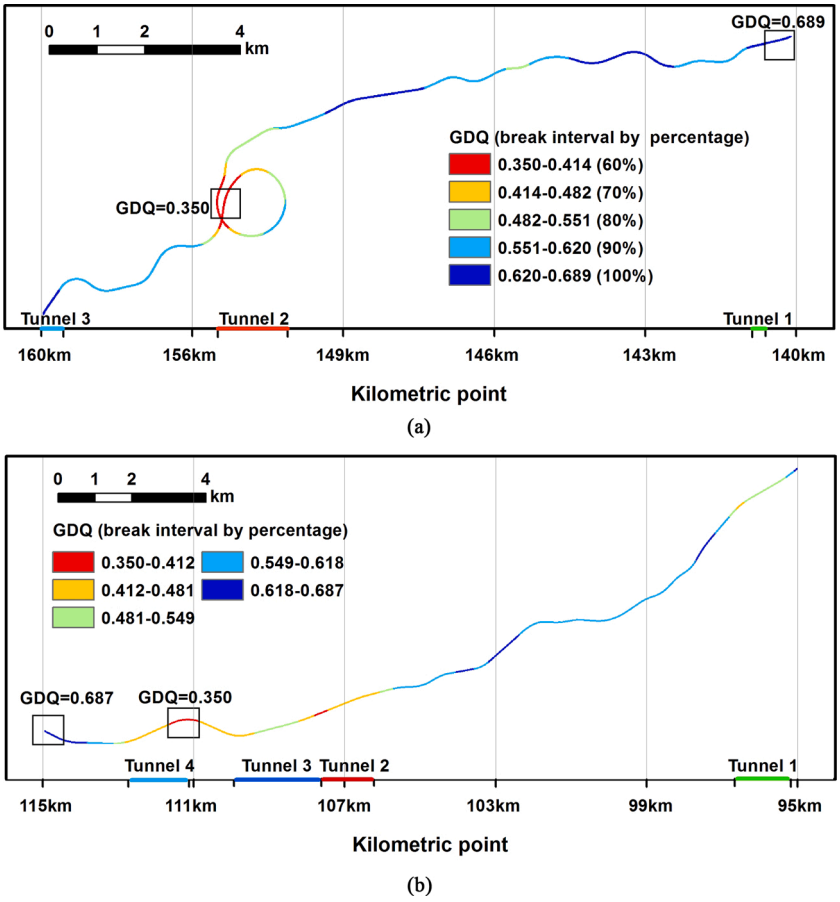

Fig. 4. GDQ spatial distribution of (a) Case 1 and (b) Case 2.

Table 5
NB and ZINB results.

Model	Accident counts	Coefficients (B)	IRR (exp(B))	Standard error	z	P>|z|	95 % confidence interval	
NB	GDQ	−3.851	0.021	0.254	−15.15	0	−4.350	−3.353
	/lnalpha	2.784	2.784	0.187	/	/	2.416	3.151
	alpha	16.180	16.180	3.033	/	/	11.205	23.365
	AIC = 713.075							
	BIC = 723.132							
	Wald chi2(1) = 229.45 Prob > chi2 = 0							
ZINB	GDQ	−3.851	0.021	0.254	−15.16	0	−4.349	−3.353
	Inflate (constant)	−9.980	−9.980	11.389	−0.88	0.381	−32.303	12.343
	/lnalpha	2.784	2.784	0.188	14.84	0	2.416	3.151
	alpha	16.177	16.177	3.034	/	/	11.201	23.363
	AIC = 715.075							
	BIC = 730.16							
	Wald chi2(1) = 229.71 Prob > chi2 = 0							

Table 6
Poisson and ZIP results.

Model	Accident counts	Coefficients(B)	IRR (exp(B))	Standard error	z	P>|z|	95 % confidence interval	
Poisson	GDQ	−2.576	0.076	0.103	−25.10	0	−2.777	−2.375
	AIC = 1317.032							
	BIC = 1322.039							
	Wald chi2(1) = 630.25 Prob > chi2 = 0							
ZIP	GDQ	−2.576	0.076	0.103	−25.10	0	−2.777	−2.375
	Inflate (constant)	−16.364	−16.364	0.288	−56.85	0	−16.928	−15.800
	AIC = 1319.032							
	BIC = 1329.046							
	Wald chi2(1) = 630.24 Prob > chi2 = 0							

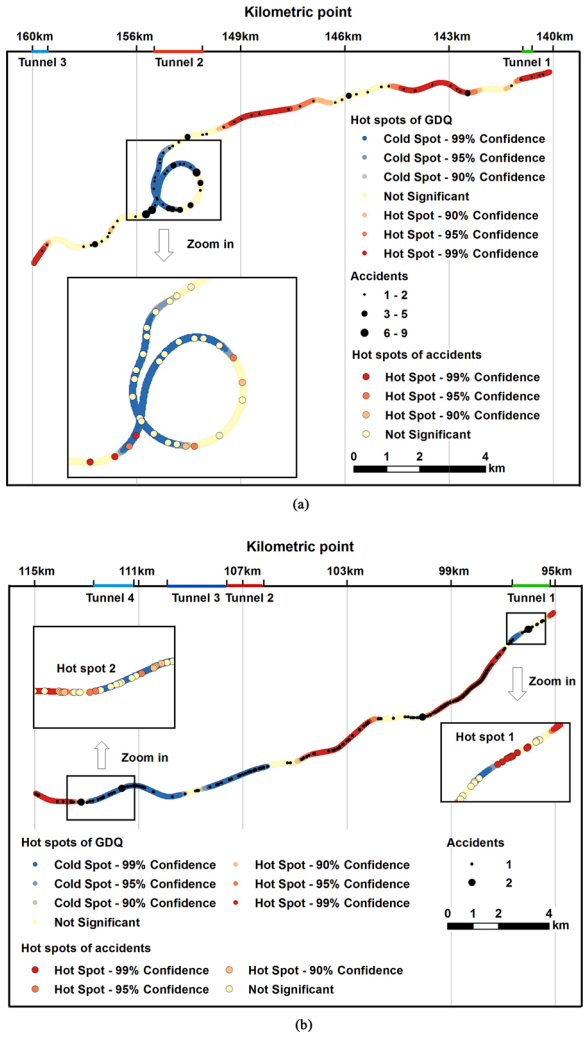

Fig. 5. Hot spot analysis for Case 1 (a) and Case 2 (b).

km, 142.26 and 144.28 km, 147.08 and 148.96 km, and 159.46 and 160 km. While the longitudinal grade and horizontal/vertical alignment change of these areas were relatively small, their curve radii projected to the horizontal plane were relatively large.

In Case 2, lower GDQ values existed in between 106.76 and 108.78 km and 109.9 and 113.06 km. The lowest GDQ value was 0.35 and appeared at the 111.58 km kilometric point, i.e., the tunnel 4 entrance. Its curve radius projected to the horizontal plane was 850 m and its vertical alignment change was 2.878 %. Higher GDQ values appeared in between 95 and 95.34 km, 97.54 and 98.28 km, 103.08 and 104.86 km, and 113.96 and 115 km. Likewise, the longitudinal grade and horizontal/vertical alignment change of these areas were relatively small whereas their curve radii projected to the horizontal plane were relatively large.

In Case 1, the road lengths represented as the 60th, 70th, 80th,90th, and 100th GDQ percentiles accounted for 10.6 %, 5.8 %, 14.2 %, 43 % and 26.4 %, indicating more than 15 % of the areas scored relatively lower GDQ. In Case 2, the percentiles accounted for 5.1 %, 21.5 %, 14.9 %, 42.3 % and 16.2 %, indicating more than 25 % of the areas scored relatively lower GDQ.

3.3. Analysis of the GDQ and accidents

3.3.1. Regression analysis

In Case 1, Negative Binomial Regression (NB) and Zero-inflated Negative Binomial Regression (ZINB) were used to understand the relationship of GDQ and accidents. According to the NB and ZINB results (Table 5), a 95 % confidence interval of the overdispersion parameter alpha was between 11.205 and 23.365, indicating that the null hypothesis of "alpha = 0" (corresponding to Poisson Regression) was rejected, and the NB model was better than the Poisson Regression model. The Wald test also showed that the null hypothesis was rejected (Prob > chi2 = 0) and the explanatory variables needed to be included in the NB and ZINB models. Besides, the NB model had smaller Akaike information criterion (AIC) and Bayesian information criterion (BIC) values, which fit the data better than the ZINB model (AIC = 713.075 < 715.075, BIC = 723.132 < 730.16) (Wilson, 2015). The NB results showed that while the covariate constants remained unchanged, the Incidence Rate Ratio (IRR), also known as exp(B), received a scoring of 0.021. This means improving the GDQ can contribute to a reduced level of highway accidents.

In Case 2, the Poisson model was better than the NB model as the overdispersion parameter alpha received a score of 0. Poisson Regression and Zero-inflated Poisson Regression (ZIP) were used to examine the relationship of GDQ and accidents. Given Prob > chi2 = 0 (Table 6), the explanatory variables needed to be included in the models. Besides, the Poisson model fit the data better than the ZIP model, i.e., AIC = 1317.032 < 1319.032, BIC = 1322.039 < 1329.046. The results also showed improving the GDQ can contribute a reduced level of highway accidents.

3.3.2. Hot spot analysis (Getis-Ord Gi*)

The GDQ and accident hotspot distribution were analysed using

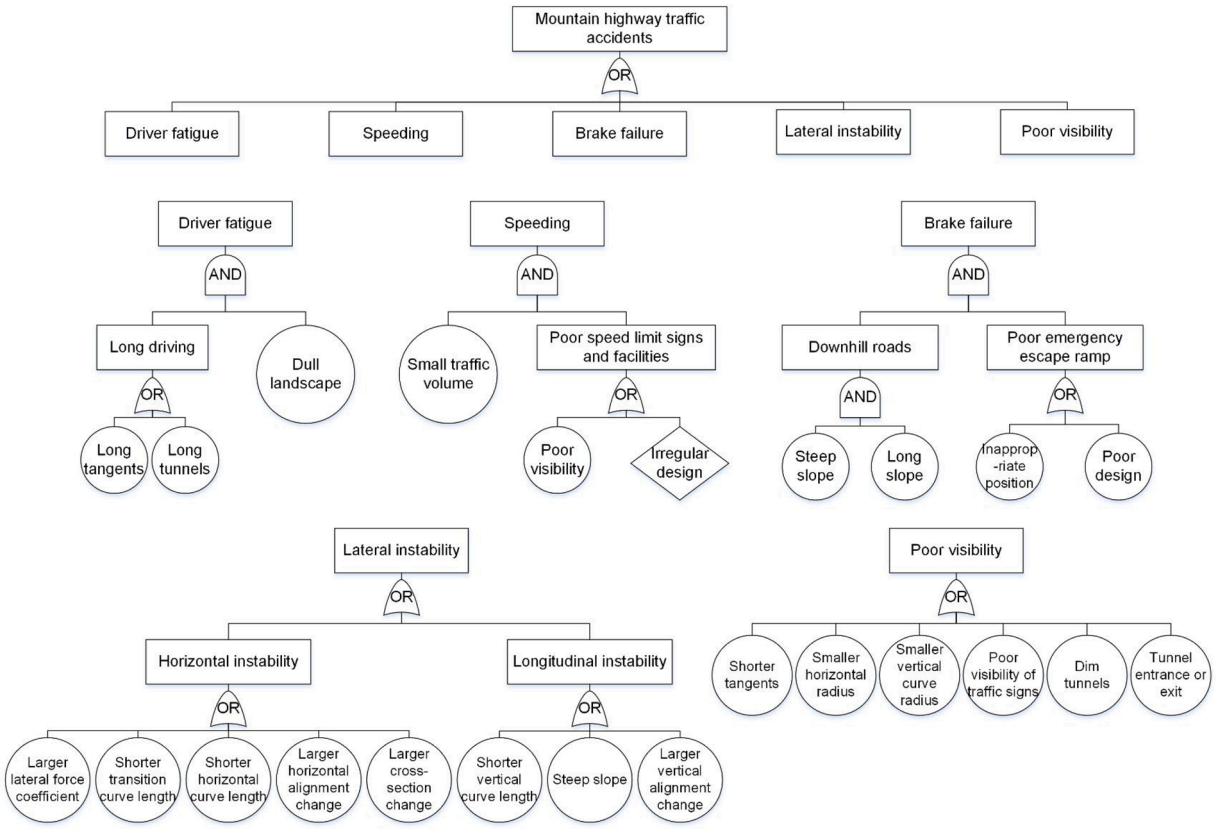

Fig. A1. Fault tree of the mountain highway traffic accidents.

Getis-Ord Gi* (Fig. 5). The results showed that the GDQ cold spots in the 90 % confidence interval were more consistent with the accident hot spots in the 95 % confidence interval. In Case 1, the GDQ cold spots were located in between 150.6 and 152.68 km and 154.14 and 156.22 km. The accident hot spots were located in between 152.7 and 152.8 km (Hot spot 1), 153.8 and 154.1 kms (Hot spot 2), and 156 and 156.6 km (Hot spot 3). Hot spot 1 was 1 km distant from the Tunnel 2 entrance. Hot spot 1's GDQ, curve radius (projected to the horizontal plane), longitudinal grade, and lateral force coefficient scored at 0.244, 629.315 m, 2.8 %, and 0.04. Both the horizontal and vertical alignment changes of Hot spot 1 were small. Hot spot 2 was about 500 m away from the Tunnel 2 exit. Hot spot 2's GDQ, curve radius (projected to the horizontal plane), longitudinal grade, and lateral force coefficient scored at 0.255, 629.315 m, 4%, and 0.04. Both the horizontal and vertical alignment changes of Hot spot 2 were large. Hot spot 3 was located at the 156 km kilometric point and possessed an emergency escape ramp. Its GDQ, curve radius (projected to the horizontal plane), longitudinal grade, and lateral force coefficient scored at 0.255, 570 m, 4%, and 0.04.

In Case 2, the GDQ cold spots in the 95 % confidence interval appeared in between 96.46 and 96.76 km, 106.76 and 108.72 km, and 109.88 and 113.06 km. There were 66 recorded accidents in these spots, accounting for 24.81 % recorded accidents. Two accident hot spots appeared in between 95.68 and 96.3 km (Hot spot 1), and 111.7 and 113.76 km (Hot spot 2), respectively. Hot spot 1 was inside Tunnel 1, and its GDQ and longitudinal grade were 0.522 and 0.5 %. Both the horizontal and vertical alignment changes of Hot spot 1 were small. Hot spot 2 was inside Tunnel 4, and its GDQ, curve radius (projected to the horizontal plane), longitudinal grade, and lateral force coefficient were 0.479, 1530 m, 1.7 %, and 0.013. Its vertical alignment change was more than 2%.

4. Discussion and conclusions

This paper presents an innovative GIS-based GDQ assessment model for optimising the vertical and horizontal alignments and improving the road traffic safety for mountainous highways. The innovation of this study can be reflected from its methodology, which has generated the mountain highway GDQ spatial distribution maps through synthetically assessing the influence of multiple risk factors related to highway design standards. In comparison, the existing research has not fully taken mountainous road design principles and design-related accidents into account, therefore, not sufficiently addressed the assessment comprehensiveness and complexity requirements. As well, the state-of-the-art assessment results are mostly qualitative rather than quantitative, for instance, the GDQ spatial distribution raster maps in this study. In the modeling process, a thorough examination of the road geometric design/design consistency related accidents led to a total of twenty identified risk factors in Table 1. The threat intensity of these twenty risk factors was also determined based on the consistent design standards, codes and regulations. Therefore, the results generated from the methodology relate to and verify the GDQ, traffic safety and design consistency requirements. This study also evidences that to the GDQ assessment, curve radius (projected to the horizontal plane), longitudinal grade, and geometric design consistency of adjacent road sections (i.e., horizontal and vertical alignment change and cross-section change) are the most influencing factors, and tunnels, sharp turns and rapid height drops typically possess lower GDQ and higher accident rates.

In Case 1, most accident hot spots possess a longitudinal grade of more than 4%. As a result, a safe design threshold is recommended at 4%. As the lower GDQ areas' vertical alignment changes would always be more than 2%, it is recommended their longitudinal grade difference be controlled to less than 2%. All these numeric implications were drawn from the case studies and in line with the existing study (Wang and Prato, 2019). Besides, enforcing speed limit in tunnels, bridges,

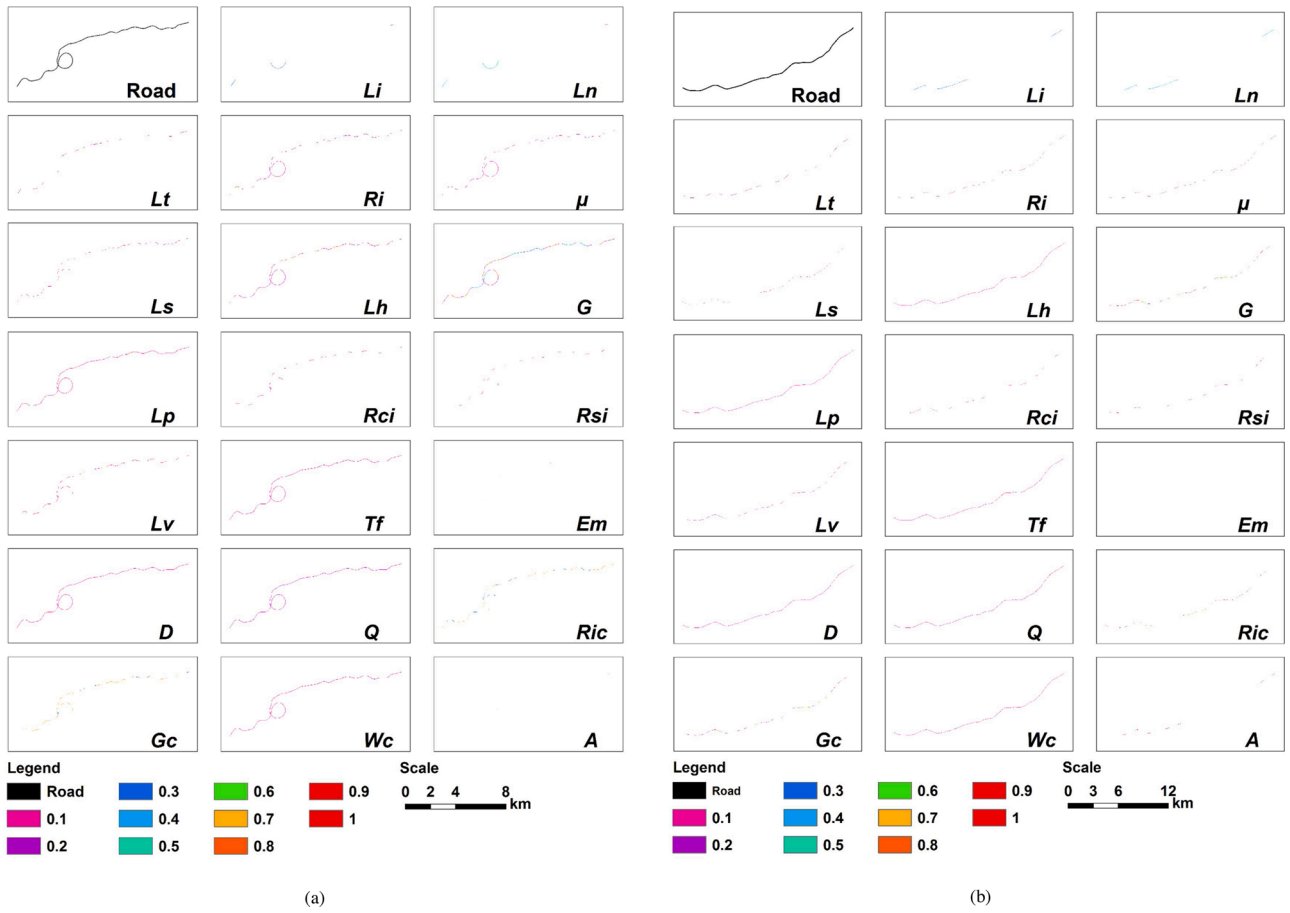

Fig. A2. Base raster map and threat raster maps of Case 1 (a) and Case 2 (b).

downhill roads, and setting emergency laybys and emergency escape ramps all could reduce the probability of accidents (Zhang et al., 2019). Overall, the methodology of this study is rational in terms of identifying and mitigating the driving risk in mountainous highways. Compared with other common methods, our methodology can take into account more assessment aspects, therefore is more comprehensive. Besides, it can generate high fidelity GDQ spatial distribution maps from GIS and does not need blind spot analysis. Last but not least, this method can be applied to different road types since the assessed risk factors and parameters are universal and easy to be adjusted.

Nevertheless, this study has some limitations. First, the model was formulated based on ecology theory, which only took into account the spatial distribution and superposition effect of various highway design risk factors. Second, vehicle condition, driver behaviour, environment impact, and broader impact synergies were not studied. Third, deriving various design parameters at different kilometric points was time-consuming and tedious. To this end, our future work will be centered around developing appropriate programs and software to improve the practicality and efficiency of the model. With the help of image recognition algorithms, genetic algorithms, and path optimisation algorithms, we will also be working towards model refinement, methodology generalisation, and intelligent transportation system design.

Author statement

The work is all original research carried out by the authors. All authors agree with the contents of the manuscript and its submission to the journal. No part of the research has been published in any form elsewhere.

Funding

This work was supported by Chang'an University (Xi'an, China) through the National Key Research & Development Program of China [grant numbers 2020YFC1512005, 2020YFC1512002], and the Science and Technology Project of Department of Transportation of Sichuan Province [grant numbers 2019-ZL-12].

Declaration of Competing Interest

The authors report no declarations of interest.

Acknowledgments

The authors would like to thank the Communication Surveying and Design Institute for providing us with the road design data of G5.

Appendix A

Table A1
Normalised risk factors and their threat intensity (adapted from AASHTO, 2018; Ministry of Transport of the People's Republic of China, 2015).

Factor	Normalised risk factors at different design speeds			Threat intensity
	120 km/h	100 km/h	80 km/h	
Li: Lighting design in tunnel	tunnel lighting reflectors only = 1			0.5~0.7
	general lighting system only = 2			0.3~0.5
	enhanced lighting system & general lighting system = 3			0.1~0.3
Ln: Tunnel length (m)	$Ln<500$			0.1
	$500\leq Ln<1000$			0.1~0.3
	$1000\leq Ln<3000$			0.3~0.5
	$Ln\geq 3000$			0.5~0.7
Lt: Tangent length (m)	$Lt<2V$ (between the curves with opposite turns)			0.5~0.7
	$2V\leq Lt<20V$ (between the curves with opposite turns)			0.1~0.3
	$Lt<6V$ (between the curves with the same turns)			0.5~0.7
	$6V\leq Lt<20V$ (between the curves with the same turns)			0.1~0.3
	$Lt\geq 20V$			0.5~0.7
Ri: curve radius (projected to the horizontal plane) (m)	$Ri<650$	$Ri<400$	$Ri<250$	1
	$650\leq Ri<1000$	$400\leq Ri<700$	$250\leq Ri<400$	0.7~0.9
	$1000\leq Ri<5500$	$700\leq Ri<4000$	$400\leq Ri<2500$	0.1~0.3
	$Ri\geq 5500$	$Ri\geq 4000$	$Ri\geq 2500$	0.1
μ: Lateral force coefficient	$\mu<0.1$			0.1~0.3
	$0.1\leq\mu<0.2$			0.3~0.5
	$0.2\leq\mu<0.35$			0.5~0.7
	$0.35\leq\mu<0.4$			0.7~0.9
	$\mu\geq 0.4$			1
Ls: Transition curve length (m)	$Ls<100$	$Ls<85$	$Ls<70$	1
	$100\leq Ls<5500$	$85\leq Ls<4000$	$70\leq Ls<2500$	0.1
	$Ls\geq 5500$	$Ls\geq 4000$	$Ls\geq 2500$	0.1~0.3
Lh: Horizontal curve length (m)	$Lh<200$	$Lh<170$	$Lh<140$	1
	$200\leq Lh<600$	$170\leq Lh<500$	$140\leq Lh<400$	0.7~0.9
	$600\leq Lh<2500$	$500\leq Lh<2500$	$400\leq Lh<2500$	0.1~0.3
	$Lh\geq 2500$	$Lh\geq 2500$	$Lh\geq 2500$	0.5~0.7
G: Longitudinal grade (%)	$0\leq G<0.3$	$0\leq G<0.3$	$0\leq G<0.3$	0.5~0.7
	$0.3\leq G<3$	$0.3\leq G<3$	$0.3\leq G<3$	0.1~0.3
	$G\geq 3$	$3\leq G<4$	$3\leq G<4$	1 (>100 km/h), 0.3~0.5 (≤100 km/h)
		$G\geq 4$	$4\leq G<5$	1 (≥100 km/h), 0.7~0.9 (<100 km/h)
			$G\geq 5$	1
Lp: Slope length (m)	$Lp<300$	$Lp<250$	$Lp<200$	1
	$300\leq Lp<700$ ($G=4\%$)	$250\leq Lp<600$ ($G=5\%$)	$200\leq Lp<500$ ($G=6\%$)	0.1~0.3
	$Lp\geq 700$ ($G=4\%$)	$Lp\geq 600$ ($G=5\%$)	$Lp\geq 500$ ($G=6\%$)	1
	$300\leq Lp<900$ ($G=3\%$)	$250\leq Lp<800$ ($G=4\%$)	$200\leq Lp<700$ ($G=5\%$)	0.1~0.3
	$Lp\geq 900$ ($G=3\%$)	$Lp\geq 800$ ($G=4\%$)	$Lp\geq 700$ ($G=5\%$)	1
		$250\leq Lp<1000$ ($G=3\%$)	$200\leq Lp<900$ ($G=4\%$)	0.1~0.3
		$Lp\geq 1000$ ($G=3\%$)	$Lp\geq 900$ ($G=4\%$)	1
			$200\leq Lp<1100$ ($G=3\%$)	0.1~0.3
			$Lp\geq 1100$ ($G=3\%$)	1
Rci: Crest curve radius projected to the vertical plane (m)	$Rci<11{,}000$	$Rci<6500$	$Rci<3000$	1
	$11{,}000\leq Rci<17{,}000$	$6500\leq Rci<10{,}000$	$3000\leq Rci<4500$	0.7~0.9
	$Rci\geq 17{,}000$	$Rci\geq 10{,}000$	$Rci\geq 4500$	0.1
Rsi: Sag curve radius projected to the horizontal plane (m)	$Rsi<4000$	$Rsi<3000$	$Rsi<2000$	1
	$4000\leq Rsi<6000$	$3000\leq Rsi<4500$	$2000\leq Rsi<3000$	0.7~0.9
	$Rsi\geq 6000$	$Rsi\geq 4500$	$Rsi\geq 3000$	0.1
Lv: Vertical curve length (m)	$Lv<100$	$Lv<85$	$Lv<70$	1
	$100\leq Lv<250$	$85\leq Lv<210$	$70\leq Lv<170$	0.7~0.9
	$Lv\geq 250$	$Lv\geq 210$	$Lv\geq 170$	0.1
Tf: Traffic engineering and roadside facilities	irregular design = 1			1
	poor visibility = 2			0.5~0.7
	standard design & good visibility = 3			0.1
Em: Emergency escape ramps	poor design = 1			1
	inappropriate position = 2			0.7~0.9
	standard design & appropriate position = 3			0.1
D: Roadside conditions	no guardrails = 1			1
	dull landscape = 2			0.3~0.5
	guardrails & nice landscape = 3			0.1
Q: Traffic volume (pcu/(h·ln))	$Q<750$	$Q<730$	$Q<700$	0.1~0.3
	$750\leq Q<1200$	$730\leq Q<1150$	$700\leq Q<1100$	0.3~0.5
	$1200\leq Q<1650$	$1150\leq Q<1600$	$1100\leq Q<1500$	0.7~0.9
	$Q\geq 1650$	$Q\geq 1600$	$Q\geq 1500$	1
Ric: Horizontal alignment change (m)	$Ric<3500$	$Ric<2500$	$Ric<1500$	0.1~0.3
	$3500\leq Ric<4500$	$2500\leq Ric<3300$	$1500\leq Ric<2100$	0.5~0.7
	$4500\leq Ric<4850$	$3300\leq Ric<3600$	$2100\leq Ric<2250$	0.7~0.9
	$Ric\geq 4850$	$Ric\geq 3600$	$Ric\geq 2250$	1

(*continued on next page*)

Table A1 (*continued*)

Factor	Normalised risk factors at different design speeds			Threat intensity
	120 km/h	100 km/h	80 km/h	
Gc: Vertical alignment change (longitudinal grade difference) (%)	$Gc<1$			0.1∼0.3
	$1\leq Gc<2$			0.5∼0.7
	$2\leq Gc<3$			0.7∼0.9
	$Gc\geq 3$			1
Wc: Cross-section change	narrowing = 1			0.5∼0.7
	widening = 2			0.3∼0.5
	no change = 3			0.1∼0.3
A: Tunnel entrance or exit	tunnel entrance = 1			0.7∼0.9
	tunnel exit = 2			0.7∼0.9

Appendix B. Supplementary data

Supplementary material related to this article can be found, in the online version, at doi:https://doi.org/10.1016/j.aap.2021.106172.

References

AASHTO, 2018. A Policy on Geometric Design of Highways and Streets, 7th edition.

Abdelrahman, A., Abu-Ali, N., Hassanein, H.S., Ieee, 2018. On the effect of traffic and road conditions on the drivers' behavior: a statistical analysis. In: 2018 14th International Wireless Communications & Mobile Computing Conference. Ieee, New York, pp. 892–897. https://doi.org/10.1109/IWCMC.2018.8450504.

Ani, M.F., Fukumi, M., RahayuKamat, S., Minhat, M., Husain, K., 2019. Development of driving fatigue strain index using fuzzy logic to analyze risk levels of driving activity. Ieej Trans. Electr. Electron. Eng. 14 (12), 1764–1771. https://doi.org/10.1002/tee.23002.

Ashley, W.S., Strader, S., Dziubla, D.C., Haberlie, A., 2015. Driving blind weather-related vision hazards and fatal motor vehicle crashes. Bull. Am. Meteorol. Soc. 96 (5), 755–778. https://doi.org/10.1175/bams-d-14-00026.1.

Budzynski, M., Kustra, W., Okraszewska, R., Jamroz, K., Pyrchla, J., 2018. The use of GIS tools for road infrastructure safety management. In: Nykiel, G. (Ed.), Seminary on Geomatics, Civil and Environmental Engineering.. E D P Sciences, Cedex A. doi:Unsp 0000910.1051/e3sconf/20182600009.

Cai, H., Lin, Y., Ieee, 2005. A preliminary study on a fuzzy driving risk model. In: Proceedings. Ieee, New YorkInternational Conference on Systems, Man and Cybernetics, Vol 1-4, pp. 1785–1790.

Chen, Fujian, Guo, Z., Chen, Fuqiang, Liu, B., 2012. Reliability design method for horizontal curve radius of highway alignment. J. Harbin Inst. Technol. 44 (04), 100–104.

Chen, Y.K., Wang, K., Xu, C.C., Shi, Q., He, J., Li, P.Q., Shi, T., 2018. Evaluation of the safety performance of highway alignments based on fault tree analysis and safety boundaries. Traffic Inj. Prev. 19 (4), 409–416. https://doi.org/10.1080/15389588.2017.1418980.

Chen, Z., Wang, X., Zhang, X., Zhang, K., 2020. Modeling of driver acceleration and deceleration behavior in mountain freeways. China J. Highw. Transp. 33 (07), 167–175. https://doi.org/10.19721/j.cnki.1001-7372.2020.07.017.

Ciobanu, S.M., Benedek, J., 2015. Spatial characteristics and public health consequences of road traffic injuries in Romania. Environ. Eng. Manag. J. 14 (11), 2689–2702.

Colonna, P., Berloco, N., Intini, P., Perruccio, A., Ranieri, V., 2016. Evaluating skidding risk of a road layout for all types of vehicles. Transp. Res. Rec. https://doi.org/10.3141/2591-11.

Colonna, P., Berloco, N., Intini, P., Ranieri, V., 2017. The method of the friction diagram: New developments and possible. In: applicationsTransport Infrastructure and Systems - Proceedings of the AIIT International Congress on Transport Infrastructure and Systems. TIS 2017. https://doi.org/10.1201/9781315281896-42.

Colonna, P., Berloco, N., Intini, P., Ranieri, V., 2020. Geometric design issues and safety analysis of two-way rural road tunnels. Transportation Research Procedia. https://doi.org/10.1016/j.trpro.2020.02.060.

Cui, Q., Wu, C., Kuang, H., 2013. Influencing factors research of airports competitiveness based BP-DEMATEL model. Syst. Eng. Pract. 33 (06), 1471–1478.

Farahmand, B., Boroujerdian, A.M., 2018. Effect of road geometry on driver fatigue in monotonous environments: a simulator study. Transp. Res. Part F-Traffic Psychol. Behav. 58, 640–651. https://doi.org/10.1016/j.trf.2018.06.021.

Hu, J., Yang, Y., Zhang, M., 2010. Safety evaluation method of combination of vertical and horizontal curves for mountainous expressway. China J. Highw. Transp. 23 (S1), 89–92. https://doi.org/10.19721/j.cnki.1001-7372.2010.s1.017.

Intini, P., Berloco, N., Ranieri, V., Colonna, P., 2020. Geometric and operational features of horizontal curves with specific regard to skidding proneness. Infrastructures. https://doi.org/10.3390/infrastructures5010003.

Kara, C., Akcit, N., 2015. Traffic accident analysis using GIS: a case study of Kyrenia City. In: Hadjimitsis, D.G., Themistocleous, K., Michaelides, S., Papadavid, G. (Eds.), Third International Conference on Remote Sensing and Geoinformation of the Environment doi:95351410.1117/12.2192435.

Li, P.Q., He, J., 2016. Geometric design safety estimation based on tire-road side friction. Transp. Res. Part C-Emerg. Technol. 63, 114–125. https://doi.org/10.1016/j.trc.2015.12.009.

Li, C.Q., Ding, L.Y., Zhong, B.T., 2019. Highway planning and design in the Qinghai-Tibet Plateau of China: a cost-safety balance perspective. Engineering 5 (2), 337–349. https://doi.org/10.1016/j.eng.2018.12.008.

Lipovetsky, S., 2010. Double logistic curve in regression modeling. J. Appl. Stat. 37 (11), 1785–1793. https://doi.org/10.1080/02664760903093633.

Llopis-Castello, D., Findley, D.J., Camacho-Torregrosa, F.J., Garcia, A., 2019. Calibration of inertial consistency models on North Carolina two-lane rural roads. Accid. Anal. Prev. 127, 236–245. https://doi.org/10.1016/j.aap.2019.03.013.

Luque, R., Castro, M., 2016. Highway geometric design consistency: speed models and local or global assessment. Int. J. Civ. Eng. 14 (6A), 347–355. https://doi.org/10.1007/s40999-016-0025-2.

Ma, Y.L., Qi, S.M., Fan, L.Y., Lu, W.X., Chan, C.Y., Zhang, Y.P., 2019. Dynamic Bayesian network approach to evaluate vehicle driving risk based on on-road experiment driving data. IEEE Access 7, 135050–135062. https://doi.org/10.1109/access.2019.2941959.

Meng, X., Guan, Z., Zheng, L., 2011. Safety evaluation of mountainous expressway based on geometric alignment indexes. China J. Highw. Transp. 24 (02), 103–108. https://doi.org/10.19721/j.cnki.1001-7372.2011.02.017.

Meng, X., Zhang, X., Zheng, L., 2012. Prediction of rear-end collisions on mountainous expressway based on geometric alignment and traffic conditions. China J. Highw. Transp. 25 (04), 113–118. https://doi.org/10.19721/j.cnki.1001-7372.2012.04.016.

Ministry of Transport of the People's Republic of China, 2015. Technical Standard of Highway Engineering. JTG, pp. B01–2014.

Mulder, C., Hendriks, A.J., 2014. Half-saturation constants in functional responses. Glob. Ecol. Conserv. 2, 161–169. https://doi.org/10.1016/j.gecco.2014.09.006.

Naji, H.A.H., Xue, Q.J., Lyu, N.C., Wu, C.Z., Zheng, K., 2018. Evaluating the driving risk of near-crash events using a mixed-ordered logit model. Sustainability 10 (8), 20. https://doi.org/10.3390/su10082868.

Naji, H.A.H., Xue, Q.J., Zheng, K., Lyu, N.C., 2020. Investigating the significant individual historical factors of driving risk using hierarchical clustering analysis and Quasi-Poisson regression model. Sensors 20 (8), 20. https://doi.org/10.3390/s20082331.

National Bureau of Statistics, 2019. China Statistical Yearbook (2019). China Statistics Press, Beijing.

Ping, P., Sheng, Y., Qin, W.H., Miyajima, C., Takeda, K., 2018. Modeling driver risk perception on city roads using deep learning. IEEE Access 6, 68850–68866. https://doi.org/10.1109/access.2018.2879887.

Pitaksringkarn, J., Tanwanichkul, L., Yamthale, K., 2018. A correlation between pavement skid resistance and wet-pavement related accidents in Thailand. MATEC Web of Conferences. https://doi.org/10.1051/matecconf/201819202049.

Rosey, F., Auberlet, J.M., 2012. Trajectory variability: road geometry difficulty indicator. Saf. Sci. 50 (9), 1818–1828. https://doi.org/10.1016/j.ssci.2012.04.003.

Sameen, M.I., Pradhan, B., 2017. Assessment of the effects of expressway geometric design features on the frequency of accident crash rates using high-resolution laser scanning data and GIS. Geomatics Nat. Hazards Risk 8 (2), 733–747. https://doi.org/10.1080/19475705.2016.1265012.

Shah, S.A.R., Brijs, T., Ahmad, N., Pirdavani, A., Shen, Y.J., Basheer, M.A., 2017. Road safety risk evaluation using GIS-based data envelopment analysis-Artificial neural networks approach. Appl. Sci. 7 (9), 19. https://doi.org/10.3390/app7090886.

Sun, L., You, K., 2013. Reliability-based risk analysis of vehicle moving on curved sections considering multiple failure modes. Chin. J. Highw. Transp. 26 (04), 36–42. https://doi.org/10.19721/j.cnki.1001-7372.2013.04.006.

Wang, Y.G., Prato, C.G., 2019. Determinants of injury severity for truck crashes on mountain expressways in China: a case-study with a partial proportional odds model. Saf. Sci. 117, 100–107. https://doi.org/10.1016/j.ssci.2019.04.011.

Wang, J., Wu, J., Li, Y., 2016. Concept, principle and modeling of driving risk field based on driver-vehicle-road interaction. Chin. J. Highw. Transp. 29 (01), 105–114. https://doi.org/10.19721/j.cnki.1001-7372.2016.01.014.

Wang, Z.S., Yue, Y., Li, Q.Q., Nie, K., Tu, W., Liang, S., 2017. Analyzing risk factors for fatality in urban traffic crashes: a case study of Wuhan. China. Sustain. 9 (6), 13. https://doi.org/10.3390/su9060897.

Wang, L., Yu, G.X., Wang, C.H., Yang, G.L., Yan, Z.B., 2019. Determining thresholds of traffic volume and skid resistance to reduce pavement's wet accident ratio. Chang. Daxue Xuebao (Ziran Kexue Ban) J. Chang. Univ. (Nat. Sci. Ed. https://doi.org/10.19721/j.cnki.1671-8879.2019.05.012.

Watling, C.N., Armstrong, K.A., Smith, S.S., Obst, P.L., 2016. Crash risk perception of sleepy driving and its comparisons with drink driving and speeding: which behavior

is perceived as the riskiest? Traffic Inj. Prev. 17 (4), 400–405. https://doi.org/10.1080/15389588.2015.1096350.
Wen, H., Wu, Y., Qi, W., 2016. Models of identification and formulation cause analysis on accident black spots of mountainous highway. J. Chongqing Jiaotong Univ. (Natural Sci. 35 (04) https://doi.org/10.3969/j.issn.1674-0696.2016.04.27, 137-140+151.
Wilson, P., 2015. The misuse of the Vuong test for non-nested models to test for zero-inflation. Econ. Lett. 127, 51–53. https://doi.org/10.1016/j.econlet.2014.12.029.
World Health Organization, 2015. Global Status Report on Road Safety 2015. WHO.
Wu, C.F., Lin, Y.P., Chiang, L.C., Huang, T., 2014. Assessing highway's impacts on landscape patterns and ecosystem services: a case study in Puli Township. Taiwan. Landsc. Urban Plan. https://doi.org/10.1016/j.landurbplan.2014.04.020.
Xiong, X., Chen, L., Liang, J., Cai, Y., Jiang, H., 2019. Simulation study on driving risk discrimination basedon driver's collision avoidance behavior. Automot. Eng. 41 (02) https://doi.org/10.19562/j.chinasae.qcgc.2019.02.006, 153-160+169.
Yan, Y., Sheng, Y., Yuan, H., Liu, H., 2011. Driving risk evaluation and speed control in passageway areas of freeway. J. Traffic Transp. Eng. 11 (02), 90–96. https://doi.org/10.19818/j.cnki.1671-1637.2011.02.015.
Yan, Y., Dai, Y.H., Li, X.D., Tang, J.J., Guo, Z.Y., 2019. Driving risk assessment using driving behavior data under continuous tunnel environment. Traffic Inj. Prev. 6 https://doi.org/10.1080/15389588.2019.1675154.
Yazdi, M., Khan, F., Abbassi, R., Rusli, R., 2020. Improved DEMATEL methodology for effective safety management decision-making. Saf. Sci. 127, 17. https://doi.org/10.1016/j.ssci.2020.104705.
Zainal, Z.F., Prasetijo, J., Musa, W.Z., 2017. Road service performance based on integrated road design consistency (IC) along Federal Road F0023. In: Zainorizuan, M.J., Yong, L.Y., Siang, L., Hanifi, O.M., Nazahiyah, R.S., Shalahuddin, A.M. (Eds.), International Symposium on Civil and Environmental Engineering 2016. doi:Unsp 0801310.1051/matecconf/201710308013.
Zhang, Q., 2020. Research on safety evaluation method of tunnel visual environment. IOP Conf. Ser. Mater. Sci. Eng. 741 https://doi.org/10.1088/1757-899x/741/1/012084, 012084 (9 pp.)-012084 (9 pp.).
Zhang, C., Meng, L., Wang, S., Chen, J., Shao, D., 2015a. Sideslip risk simulation analysis of passenger car braking behavior on expressway curved sections. China J. Highw. Transp. 28 (12), 134–142. https://doi.org/10.19721/j.cnki.1001-7372.2015.12.019.
Zhang, C., Shao, D., Zhang, M., 2015b. Risk analysis of passenger car moving on curved sections based on sideslip microscopic simulation. J. Syst. Simul. 27 (07), 1609–1616. https://doi.org/10.16182/j.cnki.joss.2015.07.027. +1627.
Zhang, W., Ma, J., Luo, W., Li, D., Li, Z., 2016. Identification model for risk level of traffic accident section based on extension science. J. Chongqing Jiaotong Univ. (Natural Sci. 35 (01), 107–110. https://doi.org/10.3969/j.issn.1674-0696.2016.01.21.
Zhang, C., Gong, Q., Liu, Y., Yan, J., Zhang, M., 2017. Computing a ground appropriateness index for route selection in permafrost regions. J. Traffic Transp. Eng. (English Ed. https://doi.org/10.1016/j.jtte.2017.07.006.
Zhang, C., Hou, Y., Qin, J., Zhang, H., 2019. Safety design method of long slope downhill slope based on temperature increase of brake drum. J. South China Univ. Technol. (Nat. Sci. Ed.) 47 (10), 139–150. https://doi.org/10.12141/j.issn.1000-565X.190077.
Zhang, H., Zhai, Y., Zhang, C., Sun, B., Xiang, Y., Hu, R., 2020a. A GIS-based Method for Driving Risk Evaluation.
Zhang, H., Zhang, C., Hu, T., Zhang, M., Ren, X., Hou, L., 2020b. Exploration of roadway factors and habitat quality using InVEST. Transp. Res. Part D Transp. Environ. 87, 102551 https://doi.org/10.1016/j.trd.2020.102551.